Available online at www.sciencedirect.com
SCIENCE DIRECT®
Journal of Power Sources 139 (2005) 295–303
JOURNAL OF POWER SOURCES
www.elsevier.com/locate/jpowsour

Differential voltage analyses of high-power, lithium-ion cells 1. Technique and application☆

Ira Bloom*, Andrew N. Jansen, Daniel P. Abraham, Jamie Knuth, Scott A. Jones, Vincent S. Battaglia, Gary L. Henriksen

Electrochemical Technology Program, Argonne National Laboratory, 9700 South Cass Avenue, Argonne, IL 60439, USA

Received 28 June 2004; accepted 20 July 2004
Available online 16 September 2004

Abstract

The *C*/25 discharge data from 18650-size cells containing $LiNi_{0.8}Co_{0.1}Al_{0.1}O_2$ cathode and graphite anode laminates were analyzed through the use of the differential voltage, d*V*/d*Q*, curves. Using half-cell data, the peaks in the d*V*/d*Q* curve of the full cell data were assigned. Analysis of the relative peak shifts allowed for the determination of the source of capacity fade. For cells formed and aged at 45 °C for 40 weeks (capacity fade = 7.5%), the analysis indicated negligible loss of accessible material at the anode and at the cathode. Capacity loss of the cell could be accounted for, largely, by side reactions at the anode. This type of analysis can be used when the introduction of a reference electrode is difficult or impractical.

Keywords: Differential voltage; Reference electrode; Lithium ion; Battery

1. Introduction

Lithium-ion batteries have attracted much interest since the initial report in the early 1990s [1]. These batteries usually consist of a lithiated metal oxide positive electrode (cathode), such as $LiCoO_2$, $LiMn_2O_4$, or $LiNiO_2$, a carbon negative electrode (anode) and a lithium salt dissolved in an organic electrolyte. Lithium-ion batteries have found many uses in consumer electronics. Such batteries are also being considered for use in automotive applications by the U.S. Department of Energy and automobile manufacturer-supported Freedom Cooperative Automotive Research (FreedomCAR) Program.

These secondary batteries operate by intercalating/de-intercalating lithium-ions in both the cathode and anode. The potential of the cell is defined by the difference in the lithium electrochemical potential between the two electrodes. Both the anode and cathode of graphite-based, Li-ion cells have potential profiles versus a lithium metal reference that vary with the amount of lithium in each electrode. Graphite intercalation is typically a first-order phase transition and consists of many potential plateaus as lithium enters or leaves the structure. Intercalation in the cathode of choice, layered oxides, exhibits typically higher-order phase transitions, in which the potential changes gradually with lithium content. Thus, the lithium content in an electrode is not only a measure of its state of charge (SOC) or discharge, but also a measure of the voltage of the electrode versus a reference electrode. Without a reference electrode, however, the cell voltage is a measure of the difference of the potentials of the cathode and anode. It does not tell the lithium content or SOC of either electrode.

☆ The submitted manuscript has been created by the University of Chicago as Operator of Argonne National Laboratory ("Argonne") under Contract No. W-31-109-ENG-38 with the U.S. Department of Energy. The U.S. Government retains for itself, and others acting on its behalf, a paid-up, nonexclusive, irrevocable worldwide license in said article to reproduce, prepare derivative works, distribute copies to the public, and perform publicly and display publicly, by or on behalf of the Government.

* Corresponding author. Tel.: +1 630 252 4516; fax: +1 630 252 4176.
E-mail address: bloom@cmt.anl.gov (I. Bloom).

0378-7753/$ – see front matter © 2004 Elsevier B.V. All rights reserved.
doi:10.1016/j.jpowsour.2004.07.021

Intercalation compounds similar to those used in the lithium-ion cell have been studied by many electrochemical techniques, such as electrochemical voltage (or potential) spectroscopy (EVS) [2–36] and galvanostatic intermittent titration [37]. A typical EVS cell consists of an intercalation compound, such as TiS_2 [2,3] or TaS_2 [4], and a counter electrode with a flat voltage profile, like lithium or sodium metal. The EVS technique uses small, discrete voltage steps while monitoring cell current. When the current reaches a low, limiting value, the cell potential is close to its equilibrium value and the voltage versus lithium content can be calculated [2,3]. EVS has been extended to a continuous voltage sweep using a very low sweep rate, $10\,\mu V\,s^{-1}$ [5,11]. Data from these measurements were used to calculate differential capacity curves (dQ/dV, approximated as $\Delta x/\Delta V$, where Δx is the number of moles or Ah of metal intercalated in a given step and ΔV is a discrete voltage change). These curves have been used to elucidate phase transitions and infer information about the mechanism of the intercalation/de-intercalation of materials into the host lattice [12–36,38].

As described above, most of the information on electrode performance is derived from well-defined electrochemical systems, in which the counter electrode maintains constant voltage during reduction and oxidation. Data from actual lithium-ion batteries can be more complex than those from, for instance, Li/TiS_2 cells. Very little information about the performance of individual lithium-ion electrodes in actual batteries is available in the literature where both electrodes' potential varies with lithium content. The full cell discharge and charge voltage versus capacity data contains thermodynamic information from both electrodes.

To separate the electrode information, one can use either dQ/dV or dV/dQ. The main difference between the two derivatives is that the peaks in the dV/dQ curve represent phase transitions, whereas the peaks in the dQ/dV curve represent phase equilibria. Graphically speaking, the approximation of dQ/dV by $\Delta x/\Delta V$, ΔV can be zero for a given Δx (e.g., in a two-phase equilibrium region); the result is division by zero, a common problem in plotting dQ/dV of graphite versus Li. dV/dQ does not have this problem since Δx, and hence, dQ, is always non-zero. The derivative of voltage with respect to capacity, dV/dQ, is well suited for graphical analysis of battery data, since the voltage of a cell can be written as

$$V_{\text{cell}} = V_{\text{cathode}} - V_{\text{anode}}$$

$(dV/dQ)_{\text{cell}}$ can be written as

$$\left(\frac{dV}{dQ}\right)_{\text{cell}} = \left(\frac{dV}{dQ}\right)_{\text{cathode}} - \left(\frac{dV}{dQ}\right)_{\text{anode}}.$$

That is, the contributions from the anode and cathode electrodes add linearly. This contrasts to the way the contributions add when using dQ/dV,

$$\left(\frac{dQ}{dV}\right)_{\text{cell}} = \frac{1}{(dV/dQ)_{\text{cathode}} - (dV/dQ)_{\text{anode}}}$$

Table 1
Cell chemistry

Cathode electrode	Anode electrode
8 wt.% PVDF binder (Kureha KF-1100)	8 wt.% PVDF binder (Kureha #C)
4 wt.% SFG-6 graphite (Timical)	92 wt.% MAG-10 (Hitachi)
4 wt.% carbon black (Chevron)	4.9 mg cm^{-2} loading density
84 wt.% $LiNi_{0.8}Co_{0.1}Al_{0.1}O_2$	35 μm-thick coating/side
8 mg cm^{-2} loading density	18 μm-thick Cu current collector
35 μm-thick coating/side	
30 μm-thick Al current collector	
Electrolyte	Separator
1.2 M $LiPF_6$ in EC/EMC (3:7 by wt.)	25 μm-thick Celgard 2325 separator

Previously, we described the results from calendar life testing at Argonne National Laboratory (ANL) under the U.S. Department of Energy's (DOE's) Advanced Technology Development (ATD) Program [39]. Here, 0.8 Ah high-power lithium-ion cells were tested using the procedures given in the PNGV Battery Test Manual [40]; in these tests, the calendar life tests were conducted at a fixed SOC. As part of the calendar life testing conducted under the ATD Program, reference performance tests (RPTs) were performed after every 4 weeks of testing. These tests are used to measure the performance of the battery with time. As part of these tests low-constant-current (C/25 rate) full charge and discharge tests were conducted to measure the amount of accessible capacity and to determine the relationship between cell potential and capacity under quasi-equilibrium conditions. Since these cells were designed for high-rate applications, the resulting charge and discharge curves contain electrode phase information with a minimum amount of kinetic artifacts and are well suited for further analyses.

Preferably, reference electrodes should be used to identify which electrode produced which part of the discharge curve as well as the source of change in a battery system as it ages. However, introducing a reference electrode into a sealed battery represents a challenge. In the present paper, we show the utility of the dV/dQ curves to identify electrode sources of capacity fade either by side reactions or loss of accessible active material.

2. Experimental

2.1. 18650-sized cells

Detailed information regarding the cell construction and the testing regime is given in [39]. The cell chemistry is given in Table 1. The cells have an average active area of 846.3 cm^2. Eleven weld-sealed 18650-sized cells were fabricated to ANL's specifications for this work. The cells underwent formation cycles at the manufacturer before delivery to

ANL. After characterization at 25 °C, one cell was removed from testing. This left 10 cells for calendar life tests at 45 °C at 60% SOC (3.741 V).

The cells were characterized in terms of their charge and discharge *C*/25 capacities before the tests began. After four weeks at temperature, the cells were cooled to 25 °C and RPTs were performed. The RPTs consisted of portions of the characterization tests, including the *C*/25 tests. The cells were then heated back to the soak temperature. The process was repeated until the power fade at the 300-Wh line was greater than 50%. See [39,41] for more information.

2.2. Half cells

Materials from fresh cells were subjected to post-test analyses. Among these analyses, small sections of the cathodes and anodes were characterized in terms of their *C*/25 capacities. Details of the post-test experiments and results will be described in a later paper [42]. The half cells consisted of 1.6 cm^2 sections of aged electrodes, new separator material, fresh electrolyte and excess lithium metal foil. The materials were assembled as button cells and cycled at room temperature between 3 and 4.3 V for the cathode and ∼50 mV and 1.5 V for the anode specimens.

The charge and discharge voltages were measured and recorded at the 30 s rate. This yielded about 2500–4800 data points for analyses. The large number of data points was needed to resolve some of the features of interest.

2.3. Data reduction and calculations

The *C*/25 charge and discharge data from the test cells as well as from the half cells were noisy due to the very slow charge/discharge rates. Mathematical filtering was used to average out the noise and accentuate the peaks. The filtering was performed using Microsoft Excel and consisted of calculating the percent depth-of-discharge (%DOD) for each point based in the experimental data and then using the FORECAST function to interpolate the cell capacity and voltage at evenly spaced %DOD intervals. Typically, 0.5% DOD intervals were used, yielding 200 points for subsequent manipulation and plotting. $-Q_0 dV/dQ$ was calculated as $-Q_0 \times \Delta V/\Delta(Ah)$, where Q_0 is the measured *C*/25 capacity of the cell, in Ah, Δ(Ah) is the change in the capacity of the cell in a given interval and ΔV is the change in cell voltage as a result of Δ(Ah). The $-Q_0$ factor served to normalize the derivatives based on cell capacity. Further smoothing of $-Q_0 dV/dQ$ was accomplished by using a 5-point moving average. Plots of $-Q_0 dV/dQ$ versus capacity density (mAh cm^{-2}) were then analyzed for trends in peak position and pattern.

Before comparing the 18650-cell and half-cell data, the 18650-cell data were shifted relative to the data from the anode half cell. The active area was also decreased. This aligned the voltage versus capacity discharge curves of the two types of cells. Once the adjustments were made, they were not changed.

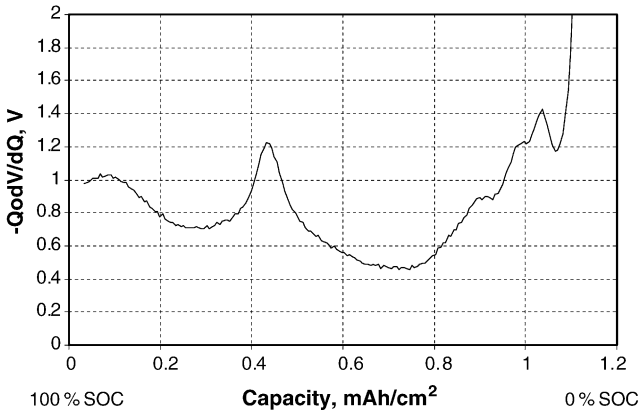

Fig. 1. A plot of $-Q_0 dV/dQ$ vs. capacity for a typical cell at $t = 0$. The SOC vs. capacity convention used in this figure is implicit for the rest of this paper.

In the analysis of the half-cell data, full-cell potentials were calculated by subtracting the anode potential from that of the cathode. Similarly, the full-cell derivative was calculated as the difference between the derivatives of the cathode and the anode. For the electrode slippage calculation (see Section 3 for a full explanation), the electrode alignments relative to each other were shifted left to right in terms of which section of the total electrode capacity was actually used in the cell. The cell capacity was defined as that between the voltage limits of 4.1 and 3.0 V.

3. Results

3.1. Half-cells

A plot of $-Q_0 dV/dQ$ versus capacity for a cell at $t = 0$ is given in Fig. 1. It contains peaks that cannot be definitively assigned without additional information. Half-cell data were used to assign the peaks in Fig. 1 to the cathode and anode. The voltage versus capacity data from an anode half-cell and a cathode half-cell can be mathematically summed to yield the voltage versus capacity behavior of the full cell. The derivative of the calculated voltage versus capacity curve should at least be qualitatively similar to that calculated from 18650 cell data. It should be noted that the half cells contained excess lithium compared with that found in an 18650 cell, and were charged and discharged beyond the voltage expected limits seen by the electrodes in a full cell; thus, the apparent capacity density of the half cells will be greater. Since the potential of lithiated graphite is about 150 mV above lithium, the cathode was charged to 4.3 V to obtain the same SOC that the cathode would see at the top of charge in a fresh 18650 cell. As a reminder, the 18650 cells that were used were cathode limited, even after formation, as is typical for Li-ion cells.

The raw voltage versus discharge capacities of the half-cell discharges for the cathode and anode, as well as their sum, are given in Fig. 2a. A comparison of the sum and

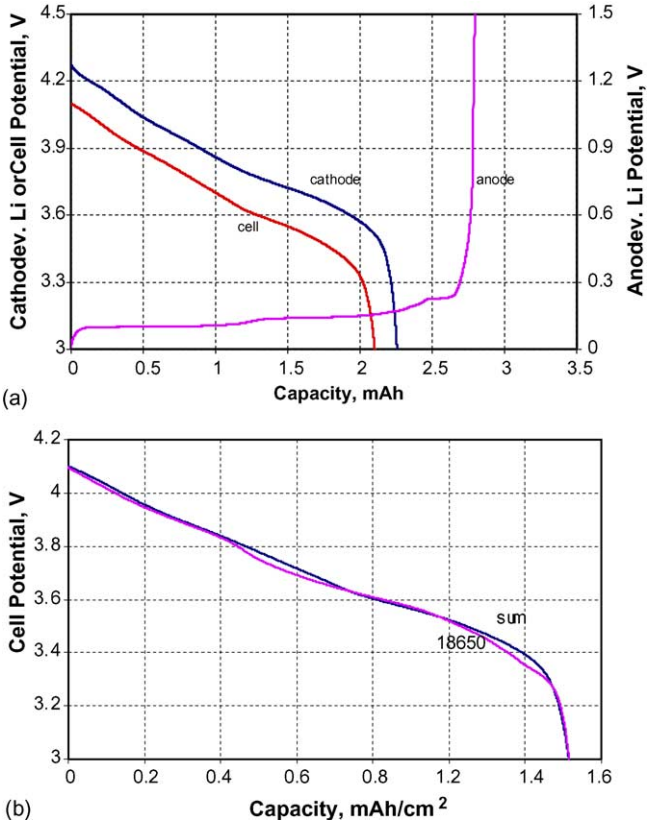

Fig. 2. (a) Calculated cell (sum of half cells) and cathode and anode half-cell potentials vs. discharge capacity. The capacity of the sum of the half cells is 2.10 mAh. (b) Cell potential vs. capacity from an 18650 cell and the sum of half cells from Fig. 2a.

the 18650 full-cell data is given in Fig. 2b. Fig. 3 shows the plots of $-Q_0 dV/dQ$ versus capacity density for anode, cathode, and sum, as well as the derivative calculated from the $C/25$ data from the 18650 cell from which the cathode and anode materials originated. From Figs. 2b and 3, however, a comparison of the sum of the half-cell data

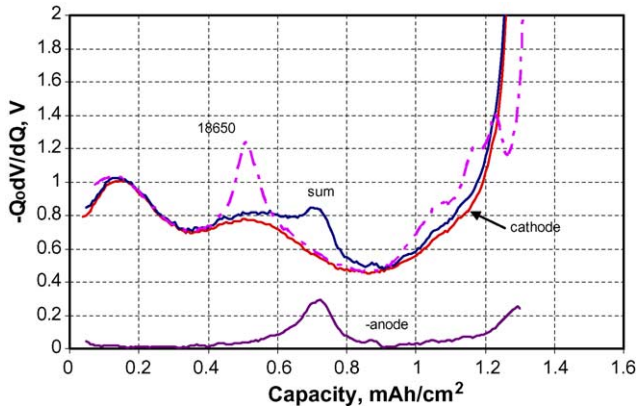

Fig. 3. $-Q_0 dV/dQ$ vs. capacity (discharge only), assuming ideal alignment, for anode and cathode half cells and their sum. The derivative calculated from the 18650 cell that was the source of the anode and cathode materials is given for comparison.

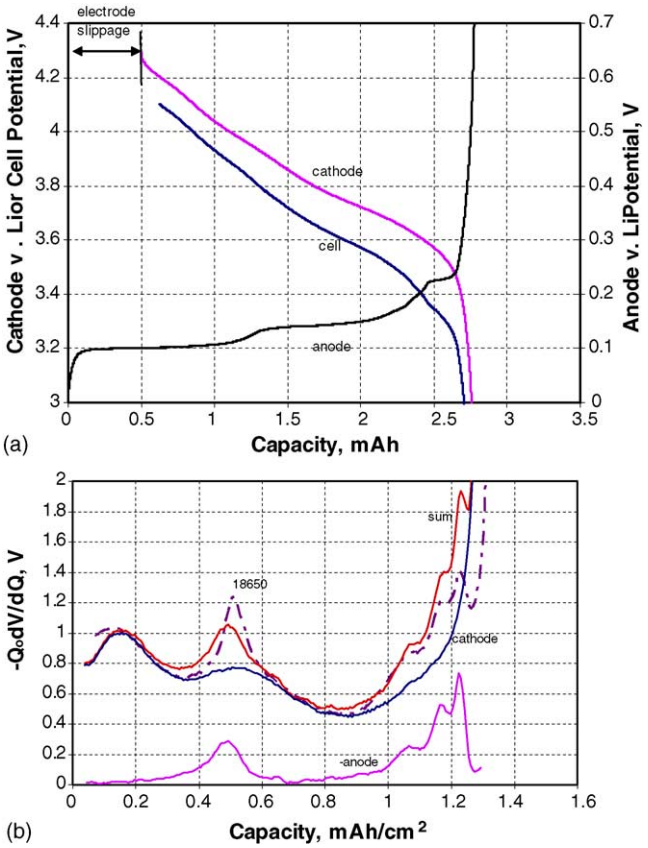

Fig. 4. (a) Effect of electrode slippage on cell voltage vs. capacity curve. The amount of electrode slippage is 0.31 mAh cm^{-2}. The calculated cell capacity is 2.08 mAh. (b) $-Q_0 dV/dQ$ vs. capacity from the data in Fig. 4a.

with the 18650-cell data shows that there are significant differences in the shape of the curves, especially in the derivative.

If the effective capacity windows of the electrodes are adjusted relative to one another (electrode slippage), the shape of the voltage versus capacity curves changes subtly. This is shown in Fig. 4a for the adjustment of 0.31 mAh cm^{-2}. (The sum of the data is not shown beyond the voltage limits of the data taken from the 18650 cells of 3.0 and 4.1 V). Comparing Fig. 4a with Fig. 2a shows that the effects of the adjustment are to decrease the usable anode capacity, utilize more of the higher-voltage section of the cathode and anode, and decrease the overall accessible capacity at the prescribed voltage limits. One also sees that the change in the sum of the curves is subtle when the curves are moved together because of the flat potential of the anode at high SOCs.

In contrast, the shape of the $-Q_0 dV/dQ$ curve changes markedly with changes in the relative movement of the half-cell data, as seen in a comparison of Figs. 3 and 4b. From the figures, one sees that as the amount of relative electrode adjustment increases, features and their positions change. An example of the complexity is the peak in the range of 1–1.4 mAh cm^{-2} that grows in as the relative electrode adjustment increases from 0 to 0.31 mAh cm^{-2} and hence its distance relative to the peak at ∼0.1 mAh cm^{-2}

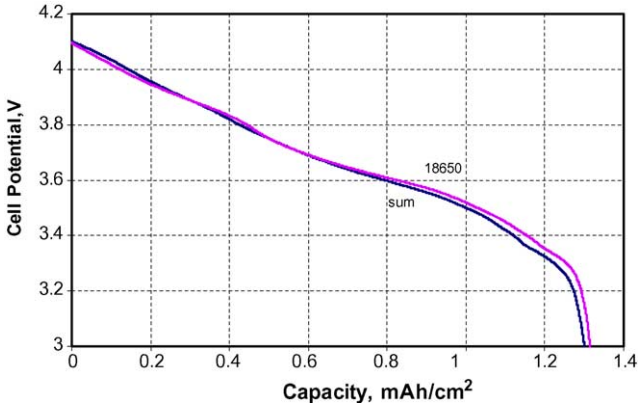

Fig. 5. The sum of half cells and 18650 cell potential vs. capacity curves. The capacity of the 18650 cell was 0.97 Ah.

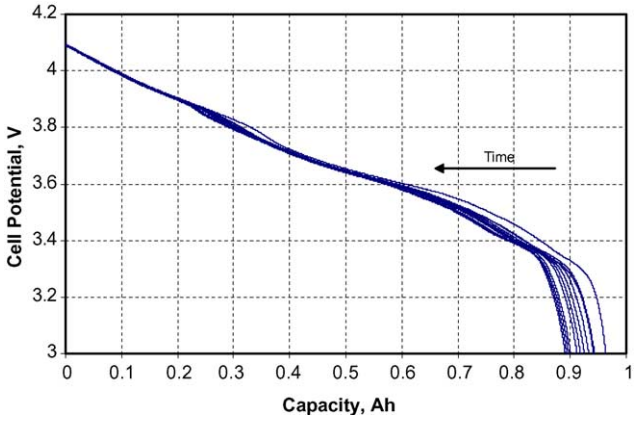

Fig. 6. Typical *C*/25 discharge voltage vs. cell capacity response as a cell ages for a calendar life cell at 45 °C. The time interval between curves is 4 weeks.

decreases. This is a result of exposure of material now being accessed at the high-voltage end of the cathode. Indeed, even the composition of the peak at ~0.1 mAh cm^{-2} changes with increasing adjustment. With no adjustment, the peak at 0.1 mAh cm^{-2} represents cathode only; at 0.63 mAh cm^{-2} adjustment, the peak represents the sum of cathode and anode peaks.

Comparing the $-Q_0 dV/dQ$ curve from the 18650 cell to that calculated (see Fig. 4b) shows that there is good qualitative agreement. Even though there is some shifting due to the differences in cell construction, all the features present in the $-Q_0 dV/dQ$ curve from the 18650 cell are present in the derived half-cell data curve. The derivatives from the cathode and anode are shown to illustrate how their derivatives contribute to the entire cell. From Fig. 4b, two out of three peaks contain contributions from both cathode and anode.

Comparing the sum of the *C*/25 discharge half-cell data shown in Fig. 4a with that from the 18650 cell (see Fig. 5) shows that there is now good agreement. The shapes of the two curves are very similar. The calculated curve has 15 μAh cm^{-2} less capacity than the 18650 curve, however, which is not significant.

With this satisfactory level of agreement, using Fig. 4b, the peaks in Fig. 1 can now be assigned. Peak 1 is from the high SOC phase transition in the cathode. Peak 2 represents contributions from both the cathode and anode, but mostly is from the mid-SOC phase transition of the anode. Peaks 3, 4, and 5 are from the low-SOC phase transitions of the anode.

3.2. 18650 cells

As the 18650 cell aged, it lost *C*/25 capacity. The typical discharge voltage versus capacity behavior as the cell aged is shown in Fig. 6. (The effect of time on the charge voltage versus capacity curve is similar and is not shown.) The initial capacity of this cell was 0.97 Ah. In a previous paper, the capacity of the cell was shown to depend on $t^{1/2}$ [39]. The cell shown in Fig. 6 exhibited 7.5% *C*/25 capacity fade after 40 weeks.

Differentiation of the discharge curves and plotting of them against capacity from the top of charge yields the curves shown in Fig. 7. From Fig. 7, it can be seen that most of the peaks in the plots shift to the left with calendar time. This is due to the aging processes that occur in the cell. It is interesting to note that Peak 1 at ~0.1 mAh cm^{-2}, which occurs at high SOC, does not shift appreciably.

As the cell ages, a new peak, labeled "2a" in Fig. 7, appears. Peak 2 separates from Peak 2a as the capacity of the cell decreases. Peak 2a appears to be "fixed" at ~0.45 mAh cm^{-2}. Comparing Fig. 7 with Fig. 4b shows that Peak 2a represents a cathode phase transition.

3.3. Analysis of 18650-cell data

Since the peaks in the $-Q_0 dV/dQ$ curve have been assigned, let us now analyze the 18650-cell data given in Fig. 7 to determine if the source of capacity fade can be identified. In this analysis we are going to classify capacity fade into two groups. The first is when there is a loss of accessible active material (LAAM) in an electrode; the second is when

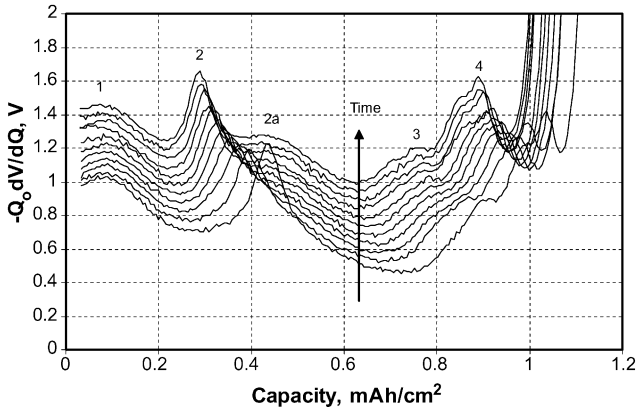

Fig. 7. The discharge-only portion of $Q_0 dV/dQ$ vs. capacity density for a calendar life cell. The time interval between curves is 4 weeks. A vertical offset was added for the sake of clarity.

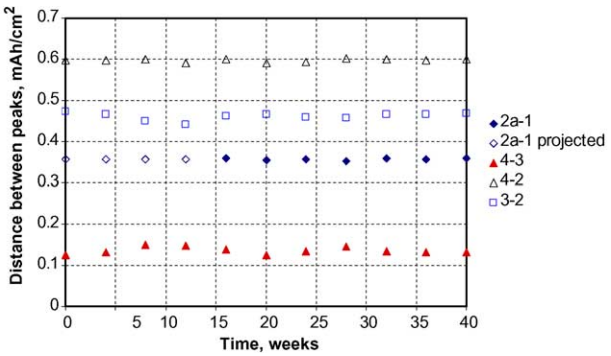

Fig. 8. Distances between peaks as a function of time. Peaks 1 and 2a are from the cathode; Peaks 2, 3, and 4 are from the anode. Cross-electrode peak distances were not calculated.

there is a shift in the alignment of the electrodes due to side reactions (SASR) at one of the electrodes. The latter source of capacity fade is equivalent to the adjustments we made above to align the electrodes with the cell data. We saw that, as the curves were brought together, the overall cell capacity would decrease without decreasing the capacity of either electrode.

The calculated distances between the cathode and anode peaks in Fig. 7 are given in Fig. 8. Part of the data for the distance between Peaks 1 and 2a is projected since Peak 2a is hard to discern at $t < 16$ weeks. From this figure, the distances between peaks do not change, within experimental error.

4. Discussion

As mentioned above, there are assumed two main reasons for capacity fade: LAAM and SASR. Examples of the two are given schematically in Fig. 9a and e, respectively, using the data from Fig. 4a.

From Fig. 9a, the capacity window starts with a large usable window between 4.1 and 3 V. If capacity is lost by LAAM, then we assume that the capacity of electrode is uniformly decreased. This also means that the capacity between $-Q_0 \mathrm{d}V/\mathrm{d}Q$ peaks is uniformly decreased, causing the peaks from the same electrode to move together with time. In the example in Fig. 9a, we assume that the capacity of the cathode is lost during the discharge uniformly; after charging back to 4.1 V, the next discharge curve would look like the "after fade" curve shown above the "before fade" curve. The new 4.1 V limit is marked as "end." Capacity loss by this route will also cause the effective discharge curve to have a higher slope and may expose new, higher-SOC cathode material for cycling, as shown in Fig. 9b, and hide some of the original high-SOC anode capacity, as shown in Fig. 9a.

Fig. 9c shows the effect of this type of capacity loss on the $-Q_0 \mathrm{d}V/\mathrm{d}Q$ curve for the entire cell. From Fig. 9d, the large peak at $\sim$0.4 mAh cm^{-2} represents the sum of cathode and anode contributions. This process can occur when the battery is being cycled or when it is at rest, as in a storage experiment. The net effect on the $-Q_0 \mathrm{d}V/\mathrm{d}Q$ curves is that the capacity window shrinks, the peaks of the affected electrode—in this case, the cathode—move closer together, and peaks of the unaffected electrode are lost at either end, as shown in Fig. 9d. A similar scheme can be envisioned for the anode.

Side reactions at an electrode consume some of its capacity in a self-discharge process. An example of this is given for side reactions on the anode in Fig. 9e. Before the reaction occurs, the usable capacity window, 4.1–3 V, is defined by the limits marked "start" in the figure. After the side reactions occur, the cathode capacity is diminished and discharge starts at a lower spot in the anode capacity window. The anode capacity is assumed to be unaffected. As the cell is purposely discharged, the voltage difference between the electrodes parallels the line marked "start" to the line marked "end." The result of this process is that, upon recharge, the anode is undercharged from its previous point. The net effect on the $-Q_0 \mathrm{d}V/\mathrm{d}Q$ curves is that peaks appear and disappear at different ends of the SOC curves. In this case, anode peaks emerge at low SOC and are lost at high SOC and vice versa for the cathode (Fig. 9f).

It is important to note that reliable half-cell data are needed for this analysis to be effective. It is also important to realize that this analysis method will not identify the capacity fade mechanism or where on the electrode voltage profile the degradation is initiated.

During the initial formation process that most Li-ion cells are put through after assembly, side reactions occur, forming the solid electrolyte interphase (SEI) layer on the anode and cathode. It is conceivable that if the formation were incomplete at room temperature, after heating the SEI layer and side reactions would progress to a more complete form. If this were to occur, one would expect to see a change in the peak pattern from the anode in the curves for t = 0,4 and 8 weeks, especially at low SOC. However, due to the nature of anode and cathode curves, the value of $-Q_0 \mathrm{d}V/\mathrm{d}Q$ from the cell is large and might mask it.

Some $-Q_0 \mathrm{d}V/\mathrm{d}Q$ curves, aligned to Peak 2, a high SOC anode peak, are shown in Fig. 10a; the same curves aligned to peak 1, a high SOC cathode peak, are given in Fig. 10b. During the first 4-week-period there is no evidence of anode peaks moving together or cathode peaks moving together; although they do appear to be moving relative to each other. This suggests that the capacity fade during the first 4-week-period is a result of SASR.

According to the discussion above, if side reactions occur at the cathode, then, at the bottom of discharge, new cathode peaks may emerge and the initial anode peaks may disappear. The opposite would be true at the top of charge. Accordingly, if side reactions occurred at the anode than at the bottom of discharge, new anode peaks might appear and initial cathode peaks would disappear. Again, the opposite would be true at the top of charge. Inspection of Fig. 10a and b strongly suggest the presence of side reac-

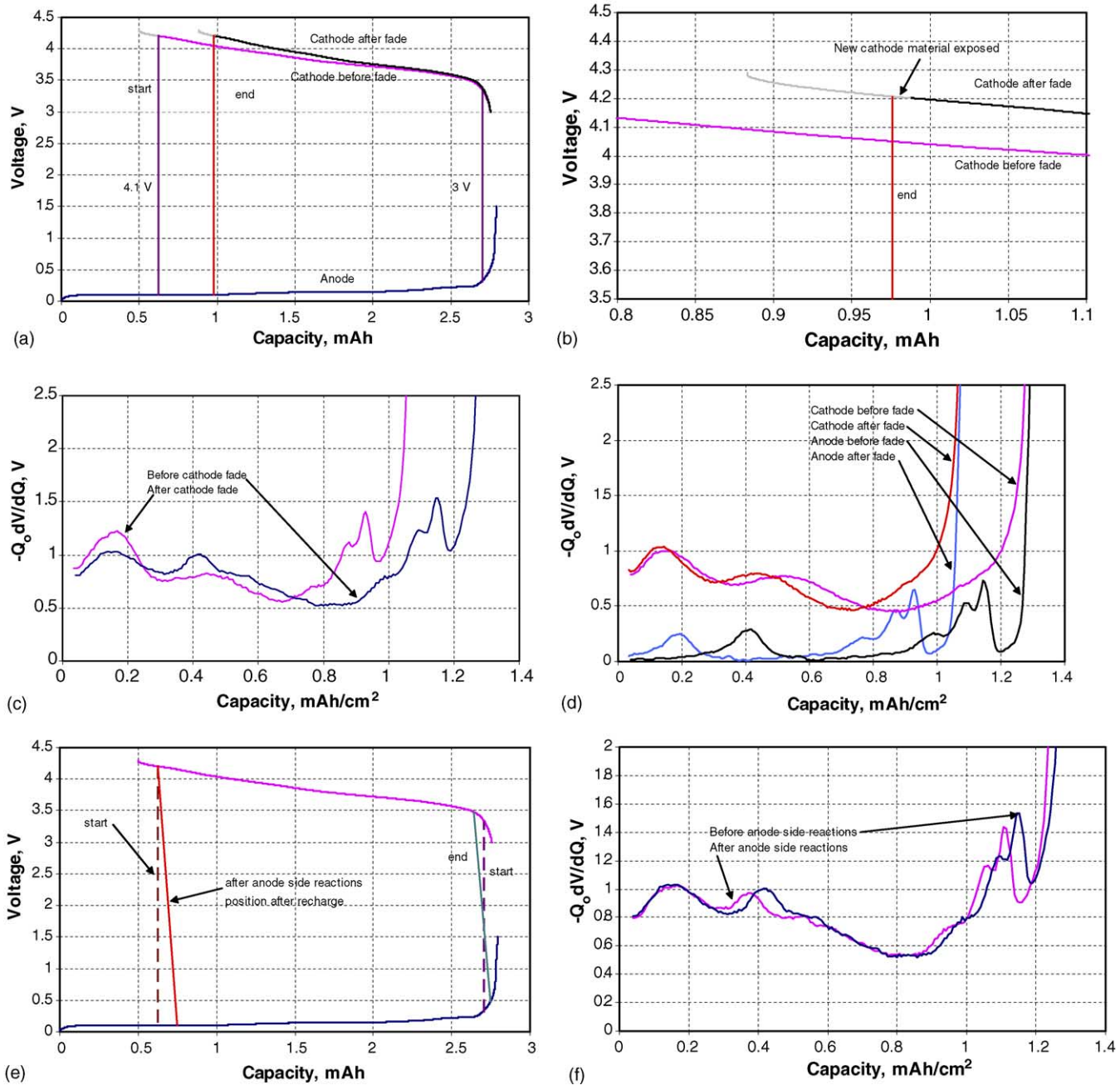

Fig. 9. (a) Capacity fades by loss of active material by, for example, particle isolation, at the cathode. In the example, a 17% capacity fade was used. The light grey sections of the cathode curves represent material that is not used during cycling. A similar process can occur at the anode. (b) Enlargement of the region around the "end" line in (a) showing new cathode material exposed due to the slight increase in potential of the anode "end point" (4.1 V cutoff is always maintained). (c) Calculated effect of cathode active material loss on $-Q_0 \mathrm{d}V/\mathrm{d}Q$ curves of the cell. (d) Calculated effect of fade by material loss or particle isolation at the cathode. The cathode peaks move closer together while the separation between the anode peaks is constant. Any signature from the anode at high SOC (low-capacity end) is lost. (e) Effect of side reactions at the anode. The dashed lines represent starting points of the usable capacity window. The side reactions occur at open circuit. Here, 6% of the anode capacity was lost in a side reaction. In this example, the anode potential is constant because it is on the phase equilibrium plateau. (f) Calculated effect of anode side reactions on the $-Q_0 \mathrm{d}V/\mathrm{d}Q$ curves of the cell. The data in figure (e) was used to calculate these curves.

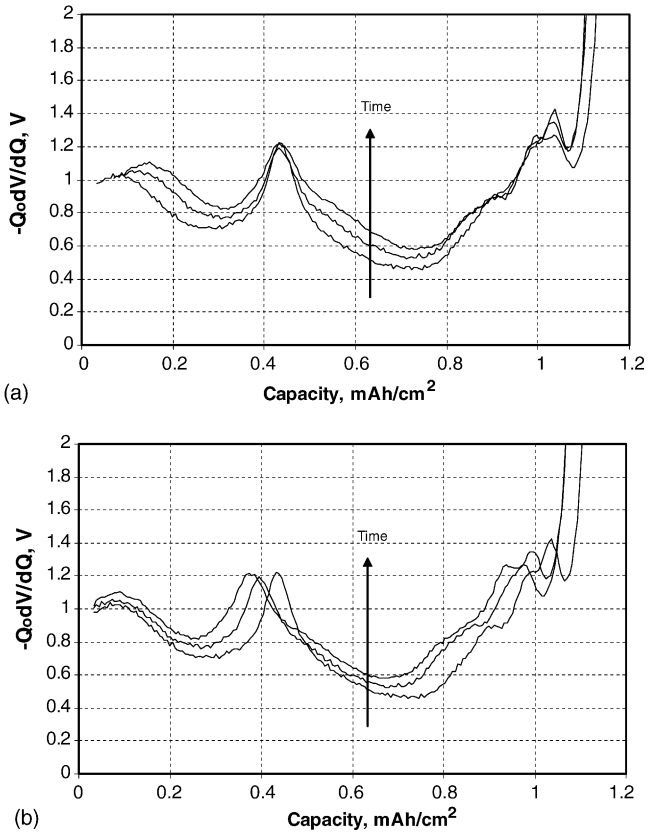

Fig. 10. Plots of $-Q_0 dV/dQ$ for t= 0, 4 and 8 weeks with (a) Peak 2 aligned. and (b) Peak 1 aligned.

tions at the anode and the incomplete formation of the SEI layer. Thus, the capacity fade is due to side reactions at the anode.

5. Conclusions

In circumstances in which the introduction of a reference electrode is not practical, much can still be gleaned from the voltage profiles of aged cells. Half-cell data from the respective electrodes can be used to identify phase transitions in full-cell data. The location of these transitions relative to one another provide insight into the source for cell capacity fade and the type of fade that is responsible for capacity loss, either loss of accessible active material or shift in alignment of electrodes due to side reactions. Applying this technique to cell data presented in an earlier publication [39] showed that the capacity fade of those cells was due to side reactions at the anode.

Acknowledgments

This work was performed under the auspices of the U.S. Department of Energy, Energy Efficiency and Renewable Energy, Office of FreedomCAR and Vehicle Technologies, under Contract No. W-31-109-Eng-38.

References

[1] O. Kazunori, M. Yokokawa, Cycle performance of lithium ion rechargeable battery, in: 10th International Seminar of Primary and Secondary Battery Technology Applications, March 1–4, 1993, Deerfield Beach, Florida, Florida Educational Seminars, Boca Raton, FL, 1993.
[2] A.H. Thompson, J. Electrochem. Soc. 126 (1979) 608.
[3] A.H. Thompson, Phys. Rev. Lett. 40 (1978) 1511.
[4] A.H. Thompson, Physica 99B (1980) 100.
[5] K. West, T. Jacobsen, B. Zacahu-Christiansen, S. Atlung, Electrochim. Acta. 28 (1983) 97.
[6] J. Barker, Synth. Met. 32 (1989) 43.
[7] J. Barker, D. Baldwin, D.C. Bott, S.J. Porter, Synth. Met. 28 (1989) 127.
[8] J. Barker, R. Pynenburg, R. Koksbang, J. Power Sources 52 (1994) 185.
[9] J. Barker, Electrochim. Acta. 40 (1995) 1603.
[10] J. Barker, M.Y. Saidi, R. Koksbang, Electrochim. Acta. 41 (1996) 2639.
[11] A. Tranchant, J.M. Blengino, J. Farcy, R. Messina, J. Electrochem. Soc. 139 (1992) 1243.
[12] D.D. MacNeil, Z. Lu, J.R. Dahn, J. Electrochem. Soc. 149 (2002) A1332.
[13] Z. Lu, J.R. Dahn, J. Electrochem. Soc. 149 (2002) A815.
[14] Z. Lu, L.Y. Beaulieu, R.A. Donaberger, C.L. Thomas, J.R. Dahn, J. Electrochem. Soc. 149 (2002) A778.
[15] P.P. Prosini, M. Lisi, D. Zane, M. Pasquali, Solid State Ionics 148 (2002) 45.
[16] H. Kim, Y.-J. Kim, D.G. Kim, H.-J. Sohn, T. Kang, Solid State Ionics 144 (2001) 41.
[17] E. Hatzikraniotis, C.L. Mitsas, D.I. Siapkas, NATO Science Series 3: High Technology 85 (2000) 529, Materials for Lithium-Ion Batteries.
[18] A. Yu, G.V. Subba Rao, B.V.R. Chowdari, Solid State Ionics 135 (2000) 131.
[19] E. Hatzikraniotis, D. Terzidis, C.L. Mitsas, D.I. Siapkas, Ionics 5 (1999) 399.
[20] J.A. Seel, J.R. Dahn, J. Electrochem. Soc. 147 (2000) 892.
[21] J.M. Paulsen, J.R. Mueller-Neuhaus, J.R. Dahn, J. Electrochem. Soc. 147 (2000) 508.
[22] Y.W. Xiao, J.Y. Lee, A.S. Yu, Z.L. Liu, J. Electrochem. Soc. 146 (1999) 3623.
[23] T. Ohzuku, Y. Iwakoshi, K. Sawai, J. Electrochem. Soc. 140 (1993) 2490.
[24] J.R. Dahn, W.R. McKinnon, J. Phys. C: Solid State Phys. 17 (1984) 4231.
[25] J.R. Dahn, W.R. McKinnon, J. Electrochem. Soc. 131 (1984) 1823.
[26] J.N. Reimers, J.R. Dahn, J. Electrochem. Soc. 139 (2091)1992.
[27] T.D. Hatchard, J.M. Topple, M.D. Fleischer, J.R. Dahn, Electrochem. Solid State Lett. 6 (2003) 129.
[28] J. Barker, M.Y. Saidi, J.L. Swoyer, Solid State Ionics 158 (2003) 261.
[29] L.Y. Beaulieu, K.C. Hewitt, R.L. Turner, A. Bonakdarpour, A.A. Abdo, L. Christensen, K.W. Eberman, L.J. Krause, J.R. Dahn, J. Electrochem. Soc. 150 (2003) A149.
[30] J. Barker, M.Y. Saidi, J.L. Swoyer, Electrochem. Solid State Lett. 6 (2003) A53.
[31] H.-Y. Lee, S.-W. Jang, S.-M. Lee, S.-J. Lee, H.-K. Baik, J. Power Sources 112 (2002) 8.
[32] A. Butz, M. Wohlfahrt-Mehrens, R. Oesten, R.A. Huggins, Ionics 2 (1996) 405.
[33] M. Wohlfahrt-Mehrens, A. Butz, R. Oesten, G. Arnold, R.P. Hemmer, R.A. Huggins, J. Power Sources 68 (1997) 582.
[34] I.A. Courtney, J.R. Dahn, J. Electrochem. Soc. 144 (1997) 2943.
[35] Y. Gao, J.R. Dahn, J. Electrochem. Soc. 143 (1996) 100.
[36] K. West, B. Zachau-Christiansen, T. Jacobsen, S. Skaarup, Electrochim. Acta 38 (1993) 1215.

[37] W. Weppner, R.A. Huggins, J. Solid State Chem. 22 (1977) 297.
[38] R. Alcántara, M. Jaraba, P. Lavela, J.L. Tirado, J. Electrochem. Soc. 151 (2004) A53.
[39] I. Boom, S.A. Jones, V.S. Battaglia, G.L. Henriksen, J.P. Christophersen, R.B. Wright, C.D. Ho, J.R. Belt, C.G. Motloch, J. Power Sources 124 (2003) 538.
[40] PNGV Battery Test Manual, DOE/ID-10597, Rev. 3, U.S. Department of Energy, February 2001.
[41] PNGV Test Plan for Advanced Technology Development Gen 2 Lithium-Ion Cells, EHV-TP-121, Rev. 6, October 5, 2001.
[42] D.P. Abraham, et al., Argonne National Laboratory, 2003, personal communication.